A Journal of the Gesellschaft Deutscher Chemiker

Angewandte International Edition

GDCh

Chemie

www.angewandte.org

Accepted Article

Title: Direct Electrochemical Ammonia Synthesis from Nitric Oxide

Authors: Jun Long, Shiming Chen, Yunlong Zhang, Chenxi Guo, Xiaoyan Fu, Dehui Deng, and Jianping Xiao

To be cited as: *Angew. Chem. Int. Ed.* 10.1002/anie.202002337
Angew. Chem. 10.1002/ange.202002337

Link to VoR: http://dx.doi.org/10.1002/anie.202002337
http://dx.doi.org/10.1002/ange.202002337

WILEY-VCH

10.1002/anie.202002337

RESEARCH ARTICLE

WILEY-VCH

Direct Electrochemical Ammonia Synthesis from Nitric Oxide

Jun Long,[+[a,b,c]] Shiming Chen,[+[a]] Yunlong Zhang,[[a]] Chenxi Guo,[[a]] Xiaoyan Fu,[[a,b,c]] Dehui Deng*[[a]] and Jianping Xiao*[[a]]

D.D. supervised the experiments and J.X. supervised all the theoretical works and conceived the project. J.L. carried out all the theoretical calculations and wrote the manuscript. S.C. carried out the experiments and wrote the experimental section of manuscript. J.L. and S.C have equal contribution. C.G. contributed to the microkinetic simulation. All the authors contributed to the data analysis and the final version of the paper.

[a] J. Long[+], S. Chen[+], Y. Zhang, C. Guo, X. Fu, Prof. D. Deng, Prof. J. Xiao
State Key Laboratory of Catalysis
Dalian Institute of Chemical Physics
Zhongshan Road 457, Dalian 116023, P. R. China.
E-mail: dhdeng@dicp.ac.cn and xiao@dicp.ac.cn
[+] These authors contributed equally to this work
[b] J. Long, X. Fu
School of Science
Westlake University
Hangzhou, 310024, P. R. China.
[c] J. Long, X. Fu
Department of Chemistry
Zhejiang University
Hangzhou 310058, P.R. China.

Supporting information for this article is given via a link at the end of the document.

Abstract: NO removal from exhausted gas is necessary due to its damage to environment. Meanwhile, the electrochemical ammonia synthesis (EAS) from N_2 is suffering from a low reaction rate and Faradaic efficiency (FE). Herein, we propose an alternative route for ammonia synthesis from exhausted NO via electrocatalysis. Density functional theory calculations indicate electrochemical NO reduction (NORR) is more active than N_2 reduction (NRR). Via a descriptor-based approach, Cu was screened out to be the most active transition metal catalyst for NORR to NH_3 due to its moderate reactivity. Moreover, kinetic barrier calculations reveal NH_3 is the most preferred product relative to H_2, N_2O and N_2 on Cu. Experimentally, a record-high EAS rate of 517.1 $\mu mol \cdot cm^{-2} \cdot h^{-1}$ and FE of 93.5% were achieved at -0.9 V vs. RHE using a Cu foam electrode, exhibiting stable electrocatalytic performances with 100 hours run. The present work provides an alternative strategy to EAS from exhausted NO, coupled with NO removal.

Introduction

Nitric oxide (NO) is one of the major air pollutants, which has caused serious environmental issues, such as acid rain, photochemical smog, and ozone depletion. The NO pollutant mainly comes from the combustion of fossil fuels in power plants, vehicles and factories[1]. At present, the most popular way of NO removal is the selective catalytic reduction (SCR) technology, by which NO can be converted into harmless nitrogen (N_2) and released[2]. However, it's not the ideal way because it will consume valuable ammonia (NH_3) or hydrogen (H_2) as the reductant. In the meanwhile, the artificial N_2 fixation to NH_3 is another challenged chemical process. As an essential chemical substance to produce fertilizers, NH_3 was mainly produced via Haber-Bosch process in industry, while it suffers from a high temperature of 300~500 ℃ and pressure of 200~300 atm[3]. To overcome the drawbacks, electrochemical N_2 reduction reaction (NRR) has been proposed to produce NH_3 at ambient conditions[4], which mimics the biological nitrogen fixation.

Electrochemical ammonia synthesis (EAS) can be driven by renewable electrical energy, generated by solar or wind. However, two major problems limit the development of this strategy. One is the low NRR activity. The best transition metal catalysts (Ru and Mo) for NRR[4b] exhibit experimental NH_3 yield rates only 0.08 and 0.11 $\mu mol \cdot cm^{-2} \cdot h^{-1}$, respectively[4a, 5]. Another problem is the low NH_3 selectivity. For N_2 electroreduction in aqueous solution, the competing hydrogen evolution reaction (HER) is more preferred than NRR on all the transition metals due to its higher limiting potential[6]. Hence, the Faradaic efficiencies (FE) of NH_3 on pure transition metal catalysts are very low[5, 7]. Besides, an isotope labelling[8] is often needed to determine the trace amount of NH_3 production.

Although many progresses have been made recently,[9] the EAS from N_2 is still far from practice. The difficulties can be attributed to the chemical inertness of N_2 molecule. Can we directly electrochemically reduce NO from exhausted gas to ammonia by coupling NO removal and ammonia synthesis (as proposed in Scheme 1)? Is it possible to overcome the difficulties in present EAS route from N_2? In fact, electrochemical NO reduction reaction (NORR) has been investigated widely in nitrate, nitrite and NO conversion for wastewater treatment[10], while the catalysts were usually designed to produced N_2, instead of NH_3.

In this work, density functional theory (DFT) calculations were performed to screen an efficient NORR catalyst. It was found that Cu exhibit higher activity for NORR than NRR, as well as superior NH_3 selectivity relative to H_2 production.

Experimental study of NORR on a Cu foam electrode achieved a record-high EAS rate of 517.1 μmol·cm^{-2}·h^{-1} with a FE of 93.5% at -0.9 V vs. RHE. This work suggests an alternative EAS route from NO, coupled with NO removal, which is appealing due to the high ammonia production rate and selectivity.

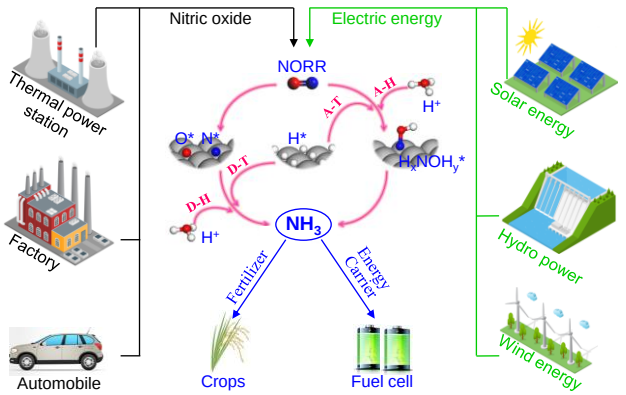

Scheme 1. Illustration of the proposed electrochemical ammonia synthesis route from NO. The nitrogen source (NO) is supposed from exhausted gases from thermal power stations, factories, or vehicles. Electrical energy can be generated from renewable solar, wind energy, or the hydro power. The produced ammonia can be used as the chemical energy carrier and feedstock of fertilizers. The middle region shows the possible reaction mechanisms (red arrows) for NORR to NH_3.

Results and Discussion

Computational screening of catalysts

According to the scaling relations of adsorption energies[11], a descriptor-based method was used in this work to screen the promising transition metal catalysts systematically. In principle, the NO reduction to NH_3 and H_2O can follow either a dissociative or associative pathway, as NRR[4b]. In the former pathway, the N-O bond can be broken at the first step. The resulting N* and O* can be then protonated, respectively. In the latter case, however, NO can be first hydrogenated to H_xNOH_y intermediates, which will be continually reduced to NH_3 and H_2O. For each pathway, the hydrogenation process can either undergo a Tafel-type route, namely, where the solvated protons first adsorb on catalysts forming adsorbed H*, followed by surface hydrogenation, or a Heyrovsky-type route, where a NO molecule and intermediates are protonated directly. Consequently, there are four categories of NORR mechanisms including dissociative-Tafel (D-T), Heyrovsky (D-H), associative-Tafel (A-T), and Heyrovsky (A-H) mechanisms, as shown in Scheme 1 (red arrows). In addition, the A-T and A-H include four specific pathways, named distal-O, distal-N, alternating-O, and alternating-N, respectively (Figure S2). For distal-O (or N) pathway, the O (or N) atom in NO can be first hydrogenated fully to H_2O (or NH_3), followed by another atomic reduction. For the alternating-O (or N) pathway, the O and N should be hydrogenated alternately. All the considered reaction mechanisms are summarized in Table S1.

We first calculated the adsorption energies of all the intermediates involved in NORR, NRR, and HER on the terrace surfaces of 10 transition metals (see details in Figure S3 and Table S2). All the energies of intermediates show good scaling relations with N* binding energy (Figure S4). Therefore, the N* adsorption free energy [G_{ad}(N)] was chosen as the descriptor. For A-T mechanism, the four specific pathways (distal-O, distal-N, alternating-O, and alternating-N) were first studied and compared. As shown in Figure S5a~d, the ΔG-determining step (GDS) is the same ($H^+ + e^- \rightarrow H^*$) in the right leg, while different for the left leg. Among them, the alternating-N pathway is more favorable (Figure S5e), which was chosen to analyze the A-T mechanism in the following. For A-H (Figure S6), the distal-O pathway is preferred near the optimum and representative. The D-T, D-H, A-T (alternating-N pathway) and A-H (distal-O pathway) mechanisms were plotted vs. G_{ad}(N), as shown in Figure 1a~d. The activity trends among them are compared in Figure S7. As the A-H with distal-O pathway (AHDO) is more preferred as E_{ad}(N) < 2.4 eV, the NORR will be analyzed in detail for this mechanism. For AHDO (Figure 1d), as the reactivity is weak, the total reaction is limited by the NO protonation, while the NH* → NH_2* turns to be the limiting step for strong reactive metals. Among all studied transition metals, Pd and Pt are most active in D-T and A-T mechanism, while Cu is optimal in D-H and A-H (Figure 1a~d). The most important AHDO pathway for NORR to NH_3 over copper as following:

$$NO(g) + (H^+ + e^-) \rightarrow NOH^* \quad (1)$$

$$NOH^* + (H^+ + e^-) \rightarrow N^* + H_2O \quad (2)$$

$$N^* + (H^+ + e^-) \rightarrow NH^* \quad (3)$$

$$NH^* + (H^+ + e^-) \rightarrow NH_2^* \quad (4)$$

$$NH_2^* + (H^+ + e^-) \rightarrow NH_3(g) \quad (5)$$

The NRR and HER were also studied to compare with the NORR. For NRR, the associative alternating pathway is more favorable than the distal for both A-T (Figure S8) and A-H (Figure S9) mechanism. As E_{ad}(N) < -0.58 eV, the D-H mechanism is most favorable around the optimum (Figure S11). The comparison among NORR, NRR, and HER is shown in Figure 1e. A Pt was found close to the activity optimum of HER, consistent with the observed facts over transition metal catalysts for hydrogen evolution[12]. Ru and Rh are the best candidates for NRR, agreeing well with the previous study[4b]. The NRR activity is always lower than HER for all the transition metals, resulting in low NH_3 selectivity. However, the NH_3 selectivity is more preferred than HER by ~0.65 V in limiting potential for the NORR scenario, where Cu(111) is the best candidate. Furthermore, the activities of transition metal step surfaces were also studied and compared with terrace ones, as shown in Figure S12. Although the limiting step ($NH_2 \rightarrow NH_3$) for strongly reactive metals turn to be different from terrace surfaces, the Cu(211) is still close to the activity optimum. As well-known, the scaling relation of adsorption energies always limit the rate of a given chemical reaction, while the NORR activity over copper is pretty close to the activity optimum, as shown in Figure 1f. However, the NRR activities were found far from the theoretical optimum over transition metal catalysts[6].

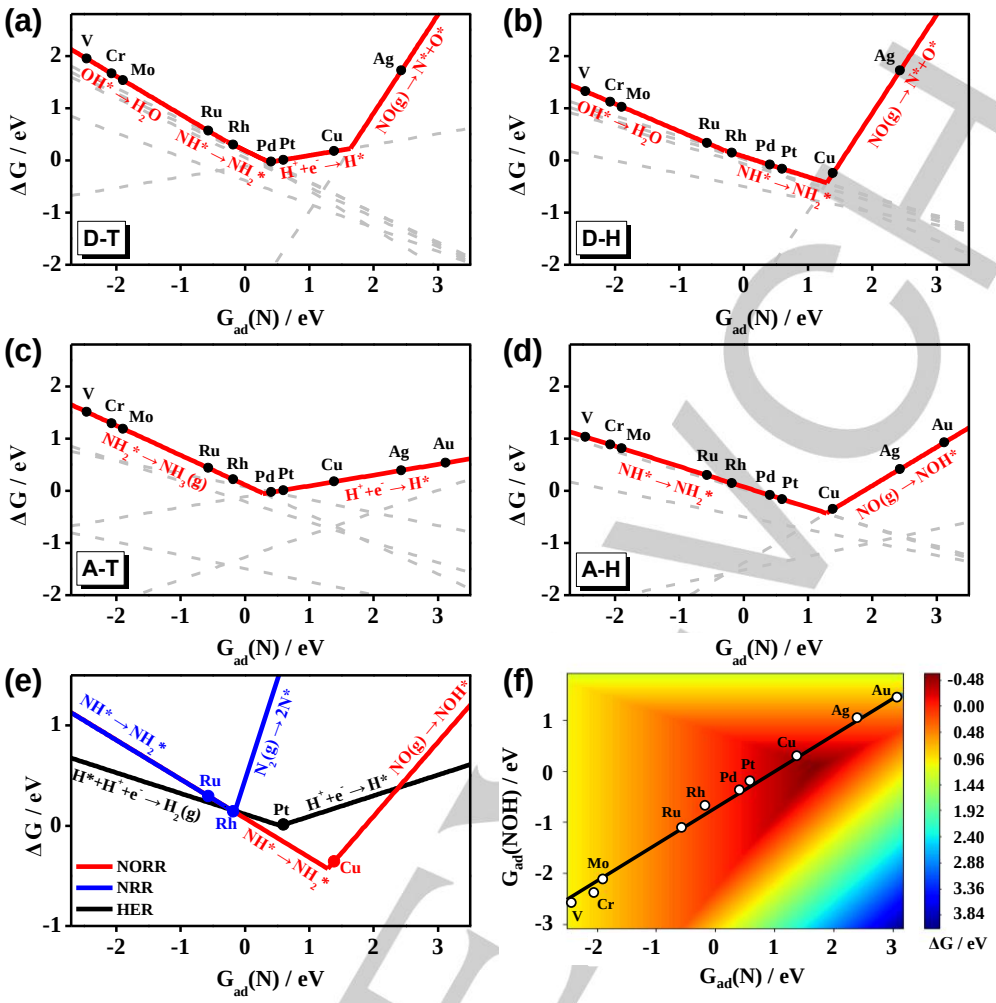

Figure 1. Thermodynamic estimation of NORR to NH_3 and screening of catalysts. (a-d) ΔG plotted versus $G_{ad}(N)$ for D-T, D-H, A-T, and A-H mechanisms, where the red and solid lines are the ΔG-limiting steps. (e) Comparison of the ΔG-determining steps between NORR, NRR, and HER. (f) A two-dimensional activity map for ammonia production. All the reaction free energies are shown at 0V vs. RHE.

NORR on Cu(111)

In this section, we will systematically study the NORR kinetics over a Cu(111) surface, combined with the calculations of potential-dependent barriers via a 'charge-extrapolation' method, proposed by Nørskov and coworkers[13]. The *ab initio* calculations of electrochemical charge transfer reactions are commonly performed at constant charge, which lead to dramatic potential shifts along the reaction path. However, the real electrochemical reactions are operated at constant potential. In finite model system, as the charge transfer (*q*) and potential (*U*) at initial (IS), transition (TS), and final state (FS) are usually correlated linearly, therefore, a capacitor model can be used to calculate the real barrier at a given potential (see Supporting Information for more details).

A layer of water with a solvated proton was added on a Cu(111) slab to explicitly model the electrochemical solid−liquid interface (Figure S13). In addition to electrochemical processes of proton transfer, some thermochemical steps are also possibly important in electrocatalysis. For example, Rosca et al.[14] proposed that a NO molecule was reduced to ammonia on Pt(100) via the pathway of NO → HNO* → NH* + O* → NH_3 + H_2O (denoted as HNO-dissociative pathway), where the HNO* dissociation is thermodynamically determined. Hence, this pathway was also explicitly studied on Cu(111), compared with the AHDO pathway. The free energy diagrams at 0 V vs. RHE and corresponding structures of IS, TS and FS are shown in Figure S14 and S15, respectively. For the HNO-dissociative pathway, the rate-determining step (RDS) is HNO* → NH* + O*, with a free energy barrier of 0.60 eV. For the AHDO pathway, the most difficult step is protonation of NOH* (0.54 eV), which is slightly lower than the former pathway and surmountable at room temperature[15]. Besides, the barrier of NOH* protonation will decrease under more negative potential in electrocatalysis, while the barrier of thermochemical HNO* dissociation remains with potential. Hence, the AHDO pathway should be more preferred on Cu(111) under experimental conditions.

According to the previous reports[10a, 16], the possible products of NORR include H_2, NH_3, N_2O and N_2. The formation of N_2O was proposed to follow a Eley–Rideal (E-R) mechanism on Pt(111)[15b], where a solvated NO first couples with an

adsorbed NO* to form a trans-ONNO* dimer (limiting step), followed by the protonation to ONNOH*. Different from Pt(111), the most difficult step of E-R mechanism on Cu(111) is the protonation of ONNOH* to form N_2O, with a barrier of 0.73 eV at 0V vs. RHE (Figure S16). Besides, the N* can be formed easily with a barrier of 0.54 eV in the AHDO pathway (Figure S14), and NH_3 is produced through the continually hydrogenation of N*. However, there are two competitive processes for N_2O (N-NO coupling) and N_2 (N-N coupling) production (Figure 2a). The limiting steps for N_2 and N_2O formation are N-N and N-NO coupling, with the barriers of 0.92 and 0.60 eV, respectively. The highest barrier to continually reduce N* to NH_3 is 0.50 eV, lower than the N-NO and N-N coupling. Moreover, the N* protonation to NH_3 is totally electrochemical reaction and the barriers will decrease at more negative potential, whereas the thermochemical N-N and N-NO coupling barriers remain intact, suggesting the NH_3 selectivity will be quite high at negative potential. In addition, the hydrogen evolution needs to overcome a barrier of 0.98 eV, which is most unfavorable compared to other products. Overall, the NORR to NH_3 should exhibit high activity and selectivity over copper electrode.

The high HER barriers compared to NH_3 production are also elucidated well. For NOH* + $(H^+ + e^-)$ → N* + H_2O, the transition states are initial-state-like (Figure 2b), resulting in a small barrier, so does the N* + $(H^+ + e^-)$ → NH* (Figure 2c). For NO + $(H^+ + e^-)$ → NOH*, NH* + $(H^+ + e^-)$ → NH_2*, and NH_2* + $(H^+ + e^-)$ → NH_3, we have analyzed the projected density of states (PDOS) and electronic localization functions (ELF) for the transition states. As the transferring protons have strong electronic interactions with O in water layer and intermediates simultaneously, as indicated by the ELF and hybridized peak α, β and γ of DOS (Figure 2d~f), suggesting the new H-O or H-N bond with adsorbates have been formed partially before H_2O···H bond breaking, which stabilize the transition states. For the proton adsorption reaction (Figure 2g), however, the H_2O···H bond has been broken before the H approaching to the surface. Therefore, the transition state is not well stabilized, and the kinetic barrier is relatively higher.

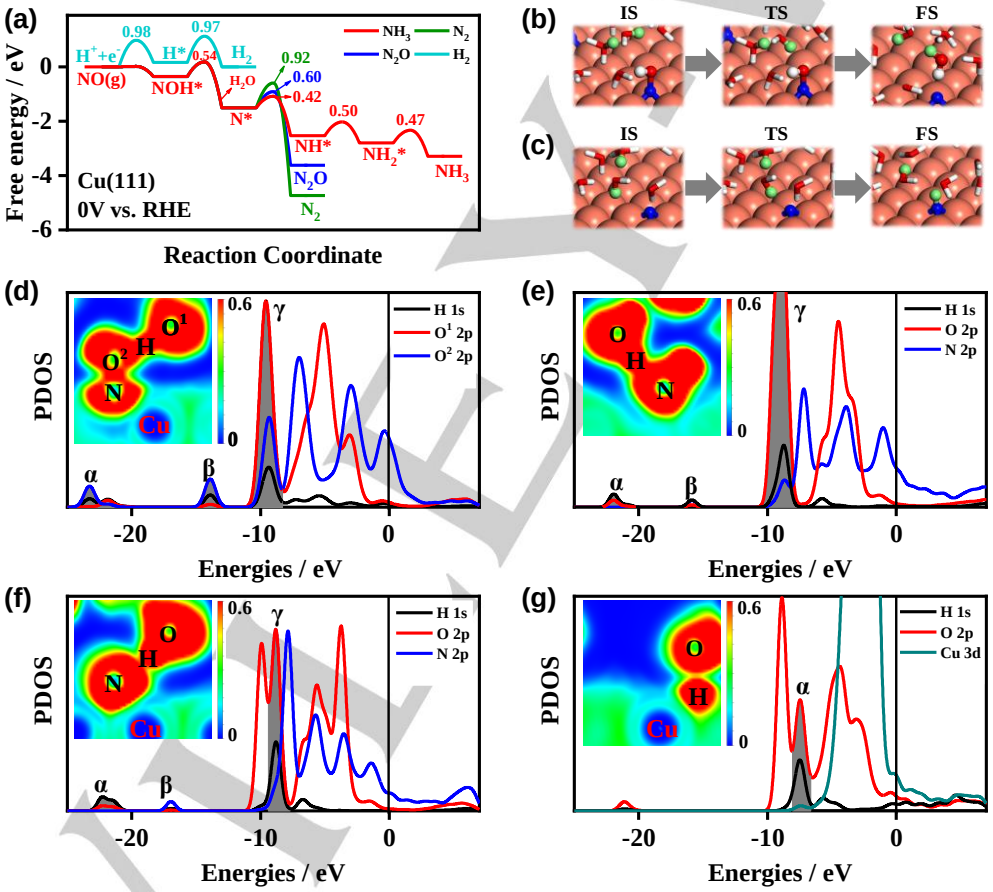

Figure 2. NORR over Cu(111). (a) Free energy diagrams for HER, NORR to NH_3, N_2O, and N_2 under 0 V vs. RHE, the kinetic barriers shown in eV. (b) Geometries of the IS, TS, and FS for NOH* + $(H^+ + e^-)$ → N* + H_2O and (c) N* + $(H^+ + e^-)$ →NH*; the light red, red, blue, and white atoms are Cu, O, N and H, respectively; the green balls represent the hydrogen participating in the proton transfer. Projected Density of States (DOS) and electron localization function (ELF) for the transition states are shown in (d) NO + $(H^+ + e^-)$ → NOH*, (e) NH* + $(H^+ + e^-)$ → NH_2*, (f) NH_2* + $(H^+ + e^-)$ → NH_3 and (g) proton adsorption.

Experimental validations

According to the theoretical calculations, copper is predicted as the most active and selective transition metal catalyst for NORR to NH_3. To confirm the prediction, we have first performed electrocatalytic NORR experiments using a Cu foil electrode at -0.9 V vs. RHE. A Pt foil was also tested for a comparison. The experiments were performed at an airtight H-shape reactor, separated by a Nafion membrane 115 at 25 ℃ for 600 s, where 0.25 mol/L Li_2SO_4 was used as electrolyte. 30 mL/min of NO flow was introduced to the cathode chamber as reactant. The

gaseous products were detected by gas chromatography (GC) and ammonia was quantified by ion chromatography (IC), details were described in Supporting Information. The NH_3 production rate on Pt and Cu foil are 99.4 and 95.0 μmol·cm^{-2}·h^{-1} (Figure 3a), respectively, which is very close. However, the H_2 evolution rate on the Pt foil (730.7 μmol·cm^{-2}·h^{-1}) is much higher than that on the Cu foil (135.7 μmol·cm^{-2}·h^{-1}) (Figure 3a), leading to the NH_3 FE of Pt foil much lower (Figure 3b). The higher current density of Pt foil than Cu foil (Figure 3c) is also attributed to the dominant HER. Hence, the Cu electrode is more interesting rather than Pt for electrochemical ammonia synthesis from NO reactant, considering the selectivity and price of catalysts. To acquire a better performance, a Cu foam catalyst was prepared and tested under the same conditions. Consequently, an excellent NH_3 formation rate (517.1 μmol·cm^{-2}·h^{-1}) and FE (93.5%) were obtained, with a significantly enhanced current density (Figure 3a~c). In addition, the overpotential for NORR on Cu foam is only 0.11 V at 10 mA·cm^{-2}, which is competitive to NRR. The improved NORR performances of Cu foam can be attributed to its porous structure, which increases the specific surface area of electrode and promotes the diffusion of NO and NH_3. In addition, the NORR performances of Cu foam were examined at different potentials (-1.2 ~ 0.3 V vs. RHE). Ammonia is always the dominant product over all studied potentials and its production rate gets higher at more negative potentials (Figure 3d). The NH_3 FE increases until the potential = -0.9 V vs. RHE (Figure 3e), with the maximum of 93.5%. Therefore, the potential -0.9 V vs. RHE was the optimal for both activity and selectivity for NORR to NH_3 over a Cu foam electrode. As a comparison, the NRR performance was also examined on the Cu foam under the same conditions at -0.9V, while only trace amount of NH_3 (< 0.1 μmol·cm^{-2}·h^{-1}) was produced (Figure 3a). Even compared with some recent NRR results (Table 1), the NORR with Cu foam still remains as a record-high EAS activity and selectivity. More strikingly, the ammonia production rate via NORR (9234 μmol·g^{-1}·h^{-1}) at ambient conditions can even reach the level of Haber-Bosch process at high temperature[17] (Table S4), suggesting EAS from NO is promising to be an alternative ammonia synthesis strategy.

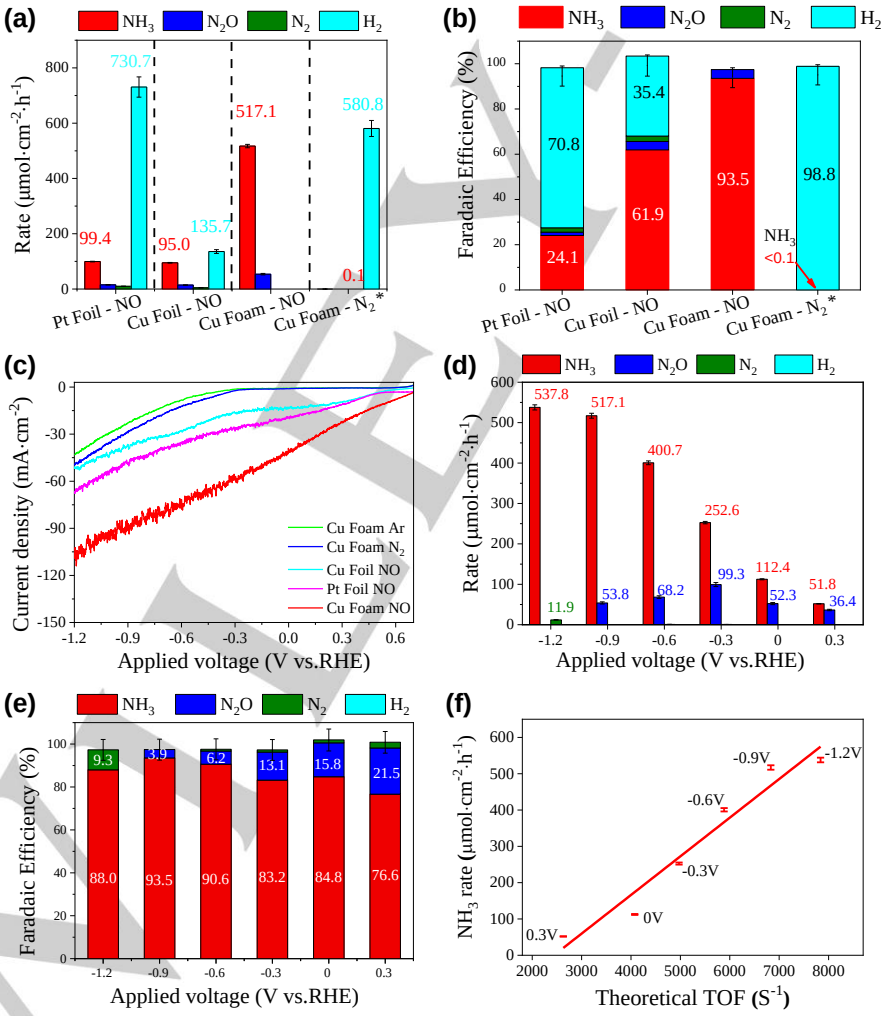

Figure 3. Experiments of NORR and NRR over different catalysts and theoretical microkinetic simulation. Reaction rate (a) and Faradaic efficiency (b) for NORR on a Pt foil, Cu Foil, and Cu foam for 600 s, and NRR over Cu foam for 2 hours at -0.9 V vs. RHE. (c) Linear Sweep Voltammetry (LSV) for Pt foil, Cu foil and Cu foam in NO-saturated 0.25 M Li_2SO_4 Cu foam in Ar or N_2 -saturated 0.25 M Li_2SO_4 acquired with a scan rate of 10 mV s^{-1} at 25 °C. Reaction rate (d) and Faradaic efficiency (e) of NORR on Cu foam at varying potentials. (f) The measured ammonia production rates over the Cu foam plotted as theoretical TOF at different potentials.

Table 1. Comparison of NORR on Cu foam with NRR from some recent reports

Catalysts	Reactants	Electrolyte	Potential (vs. RHE)	NH_3 production rate ($\mu mol \cdot cm^{-2} \cdot h^{-1}$)	FE (%)	Ref.
Ru SACs/N-C	N_2/H_2O	0.05M H_2SO_4	-0.2	1.81	29.6	[18]
Au_6/Ni	N_2/H_2O	0.05M H_2SO_4	-0.14	0.87	67.8	[9a]
Zr-TiO_2	N_2/H_2O	0.1M KOH	-0.45	0.52	17.3	[19]
K-BNC	N_2/H_2O	0.5M K_2SO_4	-0.6	52	66	[9b]
Cu foam	NO/H_2O	0.25M Li_2SO_4	-0.9	517.1	93.5	This work

Moreover, a microkinetic model was performed to estimate the turnover frequency (TOF) of NORR to NH_3 on Cu(111) under different applied potentials.[20] The kinetic equations were shown in Table 2. The reaction constant *k* is calculated following the Arrhenius-type based equation with the parameter of potential-dependent activation barriers (Equation S5). The experimental NH_3 yield rate vs. theoretical TOF was compared in Figure 3f. As the potential varying from 0.3 to -1.2 V, the TOF increases from 2630 to 7840 S^{-1}, because of the decrease of reaction and activation energies at more negative potentials. The measured NH_3 production rate exhibits a nice linear correlation with theoretically calculated activity, confirming our reaction pathways and mechanisms above.

Table 2. The kinetic equations for microkinetic model

Elementary reactions	Reaction rate (r)
$NO(g) + H^+ + e^- + * \leftrightarrow NOH*$	$r = P(NO) \cdot P(H^+) \cdot \theta(*) \cdot k_f - \theta(NOH*) \cdot k_b$ [a]
$NOH* + H^+ + e^- \leftrightarrow N* + H_2O$	$r = \theta(NOH*) \cdot P(H^+) \cdot k_f - \theta(N*) \cdot P(H_2O) \cdot k_b$
$N* + H^+ + e^- \leftrightarrow NH*$	$r = \theta(N*) \cdot P(H^+) \cdot k_f - \theta(NH*) \cdot k_b$
$NH* + H^+ + e^- \leftrightarrow NH_2*$	$r = \theta(NH*) \cdot P(H^+) \cdot k_f - \theta(NH_2*) \cdot k_b$
$NH_2* + H^+ + e^- \leftrightarrow NH_3(g) + *$	$r = \theta(NH_2*) \cdot P(H+) \cdot k_f - P(NH_3*) \cdot \theta(*) \cdot k_b$

[a] * indicates active site. θ and *P* represent the concentration and pressure of reactant, respectively. k_f and k_b are the reaction constant for forward and backward reaction, respectively.

As an isotope labelling experiment is useful to exclude the contamination of nitrogen source,[8a, 8b] we have also performed isotope labeling experiments for confirmation. ^{15}NO was used as the reactant for NORR at -0.9 V vs. RHE for 30 minutes. After reaction, the electrolyte was detected by Ion Chromatography (IC), NMR, and Indophenol blue methods independently (see details in SI). As shown in Figure 4a, a typical double peak on $^{15}NH_4^+$ at δ = 6.93 ppm and 7.04 ppm by ^{15}NO reduced product, well consistent with the $^{15}NH_4^+$ reference. Furthermore, the tipple peaks signals of $^{14}NH_4^+$ were not found on ^{15}NO reduced product, demonstrating the produced ammonia is from the NO reactant in our experiments. The quantification results are shown in Figure 4b. The average of 128.36 μmol with standard deviation of 0.098 was achieved, which indicate reliable results were obtained with the IC, NMR, and Indophenol blue Methods. In addition, a 100 hours stability test was performed for the Cu foam at -0.9 V vs. RHE (see Supporting Information for details). As shown in Figure 4c, the increment of total charge consumption was linear with time, with an average current 79 mA/cm^2. The FE of NH_3 was calculated as the average value within the measured time slot, which was always higher than 90%. The structure of the Cu foam retained after 100 hours run, according to the SEM image as shown in Figure 4d. The crystallographic structure signals after electrochemical reactions were still consistent with the XRD pattern for as-prepared samples. The diffraction peak at 2θ of 43.2^o, 50.4^o and 74.1^o correspond to the Cu(111), (200), and (220) facet, respectively. No other phases were found in the XRD patterns. The X-ray absorption near-edge structure (XANES) spectra of Cu K-edge in Cu foam before and after reaction are basically the same with the Cu foil standard, indicating the valence state of electrode is metallic Cu, as shown in Figure S23. The k^3-weighted extended X-ray absorption fine structure (EXAFS) in Figure 4e also shows the Cu-Cu coordination was dominate structure, which has been confirmed by XRD profile. Furthermore, the surface species and states over the Cu foam were studied by X-ray photoelectron spectroscopy (XPS). There are the sharp peaks at the binding energy of 933 eV and 953 eV, and no signals around 945 eV, which means the metallic Cu was dominant species on the surface. Though some Cu (II) species could be found according to the two weak satellites peaks at binding energies of 944.8 eV and 963.2 eV, which is due to the samples oxidized by air for XPS examination. However, they remain intact before and after electrochemical reactions, as shown in Figure 4f. All the characterizations above indicate the Cu foam electrode was robust enough during the 100 hours run.

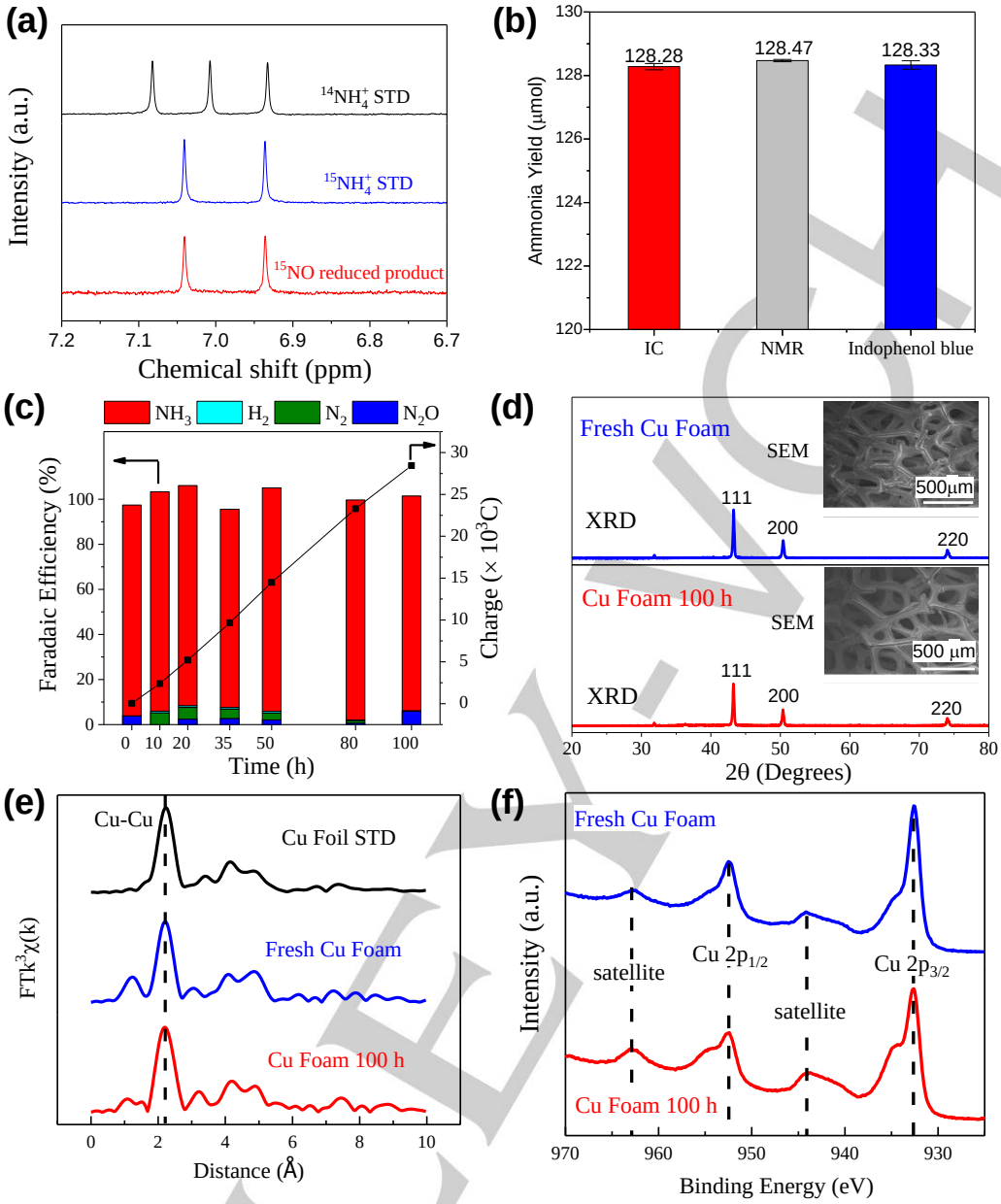

Figure 4. ^{15}NO Isotope labelling experiment, stability test and characterizations for the Cu foam electrode. (a) The ^1H NMR spectra of $^{14}NH_4^+$, $^{15}NH_4^+$ and ^{15}NO reduced product; (b) the comparison of quantification results among the Ion Chromatography (IC), NMR and Indophenol blue Methods; (c) the stability of Cu foam was examined for 100 hours at -0.9 V vs. RHE; (d) the comparison of XRD profile and SEM images for the as-prepared Cu foam samples and those after lectrochemical reactions; (e) the Fourier transforms of EXAFS signals for the standard Cu Foil samples, as-prepared Cu foam, and the Cu foam after reaction; (f) the X-ray photoelectron spectroscopy for the as-prepared Cu foam and those after reaction.

Conclusion

A new electrochemical strategy to produce ammonia from NO was proposed in this study, which can be coupled with the need of NO removal. A thermodynamic estimation based on DFT calculations suggests the NORR to NH_3 is a more effective scenario rather than NRR. Copper was screened out to be the optimal metal catalyst. Kinetic barriers calculations confirm the NH_3 selectivity over copper is greater over N_2 and N_2O production, as well as compared to hydrogen evolution. Therefore, we used the commercially available copper as electrodes in experiments and examined their electrochemical NORR performance. A record-high EAS rate (517.1 μmol·h^{-1}·cm^{-2}) and FE (93.5%) was achieved at -0.9 V vs. RHE over a Cu foam, which also showed a long-term stability for 100 hours run. Moreover, the NH_3 production rate of NORR over the Cu foam reached the level of Haber-Bosch process. Hence, we propose an alternative route for electrochemical ammonia synthesis from NO over copper, which also open up a new scenario to reuse the exhausted NO gas in industry.

Acknowledgements

This work was supported by the National Natural Science Foundation of China (No. 91945302, 21802124, 91845103, 21988101 and 21890753) , the National Key R&D Program of China (No. 2016YFA0204100 and 2016YFA0200200), Transformational Technologies for Clean Energy and Demonstration", Strategic Priority Research Program of the Chinese Academy of Sciences (No. XDA21010208), the China Postdoctoral Science Foundation Grant (No. 2019M661140), LiaoNing Revitalization Talents program (XLYC1907099) and the DNL Cooperation Fund, CAS (No. DNL180201). We thank the staff at the BL14W1 beamline of the Shanghai Synchrotron Radiation Facilities for assistance with the EXAFS and XANES measurements.

Keywords: Ammonia synthesis • NO removal • Electrocatalysis • Computational Catalyst Design

[1] T. Lee, H. Bai, *Aims Environ. Sci.* **2016**, *3*, 261-289.

[2] M. Koebel, G. Madia, M. Elsener, *Catal. Today* **2002**, *73*, 239-247.

[3] T. Kandemir, M. E. Schuster, A. Senyshyn, M. Behrens, R. Schlogl, *Angew. Chem. Int. Ed.* **2013**, *52*, 12723-12726.

[4] a) V. Kordali, G. Kyriacou, C. Lambrou, *Chem. Commun.* **2000**, 1673-1674; b) E. Skulason, T. Bligaard, S. Gudmundsdottir, F. Studt, J. Rossmeisl, F. Abild-Pedersen, T. Vegge, H. Jonsson, J. K. Norskov, *Phys. Chem. Chem. Phys.* **2012**, *14*, 1235-1245; c) C. X. Guo, J. R. Ran, A. Vasileff, S. Z. Qiao, *Energy Environ. Sci.* **2018**, *11*, 45-56.

[5] D. Yang, T. Chen, Z. Wang, *J. Mater. Chem. A* **2017**, *5*, 18967-18971.

[6] J. H. Montoya, C. Tsai, A. Vojvodic, J. K. Norskov, *ChemSusChem* **2015**, *8*, 2180-2186.

[7] a) L. Hu, A. Khaniya, J. Wang, G. Chen, W. E. Kaden, X. Feng, *Acs Catal.* **2018**, *8*, 9312-9319; b) H. Huang, L. Xia, X. Shi, A. M. Asiri, X. Sun, *Chem. Commun.* **2018**, *54,* 11427-11430; c) J. Wang, L. Yu, L. Hu, G. Chen, H. Xin, X. Feng, *Nat. Commun.* **2018**, *9*, 1795; d) M. M. Shi, D. Bao, B. R. Wulan, Y. H. Li, Y. F. Zhang, J. M. Yan, Q. Jiang, *Adv. Mater.* **2017**, *29,* 1606550.

[8] a) S. Z. Andersen, V. Colic, S. Yang, J. A. Schwalbe, A. C. Nielander, J. M. McEnaney, K. Enemark-Rasmussen, J. G. Baker, A. R. Singh, B. A. Rohr, M. J. Statt, S. J. Blair, S. Mezzavilla, J. Kibsgaard, P. C. K. Vesborg, M. Cargnello, S. F. Bent, T. F. Jaramillo, I. E. L. Stephens, J. K. Norskov, I. Chorkendorff, *Nature* **2019**, *570*, 504-508; b) J. Kibsgaard, J. K. Nørskov, I. Chorkendorff, *ACS Energy Letters* **2019**, *4*, 2986-2988; c) Y. T. Liu, D. Li, J. Yu, B. Ding, *Angew. Chem. Int. Ed.* **2019**, *58*, 16439-16444.

[9] a) Z. H. Xue, S. N. Zhang, Y. X. Lin, H. Su, G. Y. Zhai, J. T. Han, Q. Y. Yu, X. H. Li, M. Antonietti, J. S. Chen, *J. Am. Chem. Soc.* **2019**, *141*, 14976-14980; b) Y.-C. Hao, Y. Guo, L.-W. Chen, M. Shu, X.-Y. Wang, T.-A. Bu, W.-Y. Gao, N. Zhang, X. Su, X. Feng, J.-W. Zhou, B. Wang, C.-W. Hu, A.-X. Yin, R. Si, Y.-W. Zhang, C.-H. Yan, *Nat. Catal.* **2019**, *2*, 448-456; c) M. Wang, S. Liu, T. Qian, J. Liu, J. Zhou, H. Ji, J. Xiong, J. Zhong, C. Yan, *Nat. Commun.* **2019**, *10*, 341; d) Y. T. Liu, X. Chen, J. Yu, B. Ding, *Angew. Chem. Int. Ed.* **2019**, *58*, 18903-18907.

[10] a) A. C. A. D. Vooys, M. T. M. Koper, R. A. V. Santen, J. A. R. V. Veen, *Electrochimi. Acta* **2002**, *46*, 923-930; b) V. Rosca, M. Duca, M. T. D. Groot, M. T. M. Koper, *Chem. Rev.* **2009**, *109*, 2209-2244; c) H.-J. Chun, V. Apaja, A. Clayborne, K. Honkala, J. Greeley, *ACS Catal.* **2017**, *7*, 3869-3882; d) M. Duca, M. C. Figueiredo, V. Climent, P. Rodriguez, J. M. Feliu, M. T. Koper, *J. Am. Chem. Soc.* **2011**, *133*, 10928-10939.

[11] F. Abild-Pedersen, J. Greeley, F. Studt, J. Rossmeisl, T. R. Munter, P. G. Moses, E. Skulason, T. Bligaard, J. K. Norskov, *Phys. Rev. Lett.* **2007**, *99*, 016105.

[12] J. K. Nørskov, T. Bligaard, A. Logadottir, J. R. Kitchin, J. G. Chen, S. Pandelov, U. Stimming, *J. Electrochem. Soc.* **2005**, *152*, J23-J26.

[13] a) K. Chan, J. K. Norskov, *J. Phys. Chem. Lett.* **2015**, *6*, 2663-2668; b) K. Chan, J. K. Norskov, *J. Phys. Chem. Lett.* **2016**, *7*, 1686-1690.

[14] R. Victor, M. T. M. Koper, *J. Phys. Chem. B* **2005**, *109*, 16750.

[15] a) W. Hui-Fang, L. Zhi-Pan, *J. Am. Chem.Soc.* **2008**, *130*, 10996-11004; b) C. Andre, C. Hee-Joon, R. B. Rankin, G. Jeff, *Angew. Chem. Int. Ed.* **2015**, *127*, 8373-8376.

[16] A. C. A. D. Vooys, M. T. M. Koper, R. A. V. Santen, J. A. R. V. Veen, *J. Catal.* **2001**, *202*, 387-394.

[17] a) F. Chang, Y. Guan, X. Chang, J. Guo, P. Wang, W. Gao, G. Wu, J. Zheng, X. Li, P. Chen, *J. Am. Chem. Soc.* **2018**, *140*, 14799-14806; b) M. Kitano, Y. Inoue, Y. Yamazaki, F. Hayashi, S. Kanbara, S. Matsuishi, T. Yokoyama, S. W. Kim, M. Hara, H. Hosono, *Nat. Chem.* **2012**, *4*, 934-940; c) P. Wang, F. Chang, W. Gao, J. Guo, G. Wu, T. He, P. Chen, *Nat. Chem.* **2017**, *9*, 64-70.

[18] Z. Geng, Y. Liu, X. Kong, P. Li, K. Li, Z. Liu, J. Du, M. Shu, R. Si, J. Zeng, *Adv. Mater.* **2018**, 1803498.

[19] N. Cao, Z. Chen, K. Zang, J. Xu, J. Zhong, J. Luo, X. Xu, G. Zheng, *Nat. Commun.* **2019**, *10*, 2877.

[20] J.-F. Chen, Y. Mao, H.-F. Wang, P. Hu, *ACS Catal.* **2016**, *6*, 7078-7087.

10.1002/anie.202002337

Table of Contents

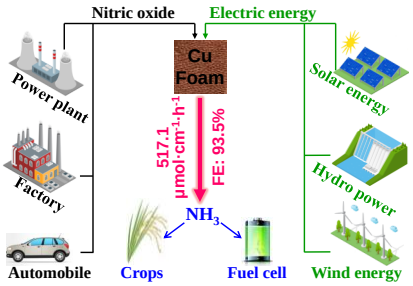

We proposed an alternative route for ammonia synthesis from exhausted NO by electrocatalysis, coupled with NO removal. A record-high electrochemical ammonia synthesis rate of 517.1 μmol·cm^{-2}·h^{-1} and FE of 93.5% were achieved at -0.9 V vs. RHE using a Cu foam electrode.